

NEAR-EXACT RADIATING FINS VIA BOUNDARY TRACING*

CONWAY LI[†], NEVILLE FOWKES[‡], BRENDAN FLORIO[§], AND MICCAL MATTHEWS[‡]

Abstract. In contexts such as space travel, thermal radiation is the primary mode of heat transfer. The Stefan–Boltzmann law gives rise to a boundary flux which is quartic in temperature, and this nonlinearity renders even the simplest of conduction–radiation problems analytically insurmountable in more than one dimension. An unconventional approach known as boundary tracing allows for analytical inroads into flux boundary value problems that would otherwise require numerical study. In this paper, the method of boundary tracing is used to generate near-exact results for an infinite family of conduction–radiation domains representing radiating fins; realistic lengths and temperatures can be realized.

Key words. boundary tracing, flux boundary condition, nonlinearity, thermal radiation

MSC codes. 35A24, 35J65, 80A20

DOI. 10.1137/22M1476228

1. Introduction. In outer space, thermal radiation is the primary means of disposing of waste heat. An archetypal steady-state problem consists of determining the temperature profile T of a conducting object Ω , with heat generated internally (or on some part of the boundary) and expelled into vacuum via radiation from its surface (Figure 1).

Assuming the object is homogeneous and isotropic, with temperature-independent thermal properties, the steady conduction within Ω is simply described by Laplace’s equation

$$(1.1) \quad \nabla^2 T = 0,$$

but on the portion of its surface $\partial\Omega$ (assumed gray and diffuse)¹ where radiation occurs, the Stefan–Boltzmann law implies that

$$(1.2) \quad \mathbf{n} \cdot \nabla T = -cT^4,$$

where

$$(1.3) \quad c = \frac{\epsilon\sigma}{k},$$

with k being the conductivity of the object, ϵ being the emissivity of its surface, and $\sigma = 5.67 \times 10^{-8} \text{ W m}^{-2} \text{ K}^{-4}$ being the Stefan–Boltzmann constant [14].

*Received by the editors February 7, 2022; accepted for publication (in revised form) May 19, 2022; published electronically July 26, 2022. This article is an abridged version of the first author’s thesis [9, mostly section 3.1].

<https://doi.org/10.1137/22M1476228>

Funding: The work of the first author was supported by an Australian Government Research Training Program (RTP) Scholarship and a Bruce and Betty Green Postgraduate Research Top-Up Scholarship.

[†]Corresponding author. Current address: RGB Assurance, Level 3, 150 St Georges Terrace, Perth, WA 6000, Australia (conwayli@pm.me).

[‡]Department of Mathematics and Statistics, The University of Western Australia, Perth, WA 6009, Australia (neville.fowkes@uwa.edu.au, miccal.matthews@uwa.edu.au).

[§]Current address: Department of Education (Western Australia), Perth, Australia (brendan.florio@uwa.edu.au).

¹i.e., a wavelength- and direction-independent emitter.

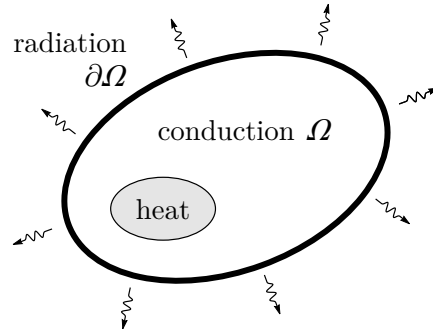


FIG. 1. *Conduction–radiation BVP with internal heat generation.*

This boundary value problem (BVP) is not straightforward even in two dimensions due to the nonlinearity of the radiation condition (1.2). The usual treatment in the literature has been to consider thin geometries for which the problem is effectively one-dimensional so that the conduction (1.1) and the radiation (1.2) may be lumped into a single ordinary differential equation (ODE) of the form

$$(1.4) \quad (\text{Derivatives of } T) - cT^4 = 0.$$

Indeed this has been the approach taken in the analytical investigations of Liu [11], Wilkins [16, 17, 18, 19], and Shouman [13] and in numerical work by Chambers and Somers [5], Lieblein [10], Bartas and Sellers [4], and Keller and Holdredge [8]. While such a simplification is an appropriate choice for the study of thin, heat-rejecting fins on spacecraft (where thinness and minimization of weight are desirable), it has also arguably been a necessity for making the BVP (1.1) and (1.2) analytically tractable; there appears to be no analytical treatment of a conduction–radiation problem in which the nonlinearity appears as a proper boundary term in the flux condition (1.2), rather than as a volumetric term in an ODE of the form (1.4). The usual procedure of separation of variables requires special geometry (Cartesian, radial, etc.), separability, and linearity. Lacking any of these it will fail, and (generally speaking) analytical solutions will not be found unless the geometry is exceptionally simple.

An alternative approach that allows for the analytical study of flux BVPs is the method of *boundary tracing*, for which a systematic framework was first devised by Anderson, Bassom, and Fowkes [2] with applications to the Laplace–Young equation of capillarity [1] and other partial differential equations, including the Helmholtz, constant mean curvature, and Poisson equations [3]. While the conventional approach fixes the domain shape and asks for a solution to the BVP, the method of boundary tracing essentially reverses this: one chooses a known exact solution to the field equation and looks for new boundaries along which the prescribed boundary condition (BC) is satisfied. Somewhat surprisingly, this procedure leads to nontrivial boundaries that can be used to produce interesting new domains which (by construction) admit the known exact solution to the BVP.

Given the relative abundance of known solutions to Laplace’s equation (1.1) and the limited amount of progress which can be made using conventional techniques for the nonlinear BC (1.2), boundary tracing is a most suitable method for tackling the conduction–radiation problem, being an analytical approach which does not require reducing the problem to one dimension. In this paper, we present the simplest case of boundary tracing in this context by using the one-dimensional solution to Laplace’s

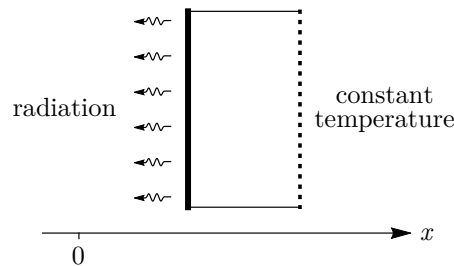


FIG. 2. One-dimensional conduction–radiation problem in a slab.

equation as the known exact solution. We show how practical, near-exact results can be produced for a family of fin-shaped domains representing radiative heat sinks.

2. Boundary tracing. The method of boundary tracing is well described by Anderson, Bassom, and Fowkes [2], but conceptually it is simple enough that one need not know the full theoretical framework to follow its application in the present paper.

In its most general form, boundary tracing can handle any BVP that couples some field equation with a flux BC of the form

$$(2.1) \quad \mathbf{n} \cdot \nabla T = F(x, y, T, \|\nabla T\|),$$

where \mathbf{n} is the outward-pointing unit normal and F is a prescribed *flux function*. One chooses a known solution T to the field equation and then seeks *traced boundaries*, which are curves consistent with the flux BC (2.1) for the chosen T . To determine the traced boundaries, one first selects an appropriate coordinate system and parametrization and then writes out the left-hand side of (2.1) in components. After solving the resulting quadratic equation (in some derivative), this results in a first-order ODE that can then be integrated to obtain the traced boundaries. These boundaries may then be used to construct new domains in which the solution to the BVP is also the chosen T .

In the case of our conduction–radiation problem, the flux BC is the radiation condition (1.2) so that the flux function is the quartic term $-cT^4$. The field equation is Laplace’s equation (1.1), and here we choose the simplest nonconstant solution,

$$(2.2) \quad T = hx,$$

corresponding to one-dimensional steady conduction with constant temperature gradient h . Such would be the equilibrium temperature profile in a slab with one face held at a fixed temperature and the other radiating into vacuum (Figure 2). The aim of boundary tracing is to look for radiation boundaries which are more interesting than a straight line (representing the flat face) but still consistent with the solution (2.2).

3. Scaling. While the known solution (2.2) is, by itself, scale-invariant with respect to both temperature and length, its coupling with the radiation BC (1.2) determines the characteristic temperature and length scales

$$(3.1) \quad \Theta = (h/c)^{1/4},$$

$$(3.2) \quad \lambda = (ch^3)^{-1/4}.$$

(In relation to the slab of Figure 2, $x = \lambda$ is the radiating face, and $T = \Theta$ its temperature.) By putting $T = \Theta \hat{T}$, $x = \lambda \hat{x}$, and $y = \lambda \hat{y}$, then dropping hats, we

eliminate the characteristic scales and reduce the boundary tracing problem to one of determining new boundaries satisfying

$$(3.3) \quad \mathbf{n} \cdot \nabla T = -T^4$$

for the chosen known solution

$$(3.4) \quad T = x$$

to Laplace's equation. In the context of thermal radiation, the temperature T is to be reckoned on an absolute scale; we will therefore ignore the region $x < 0$ in the analysis to follow, as the temperature there is negative.

4. Radiation boundaries. Selecting the parametrization $y = y(x)$ for the sought-after traced boundaries, the normal vector (up to sign) in (3.3) is given by

$$(4.1) \quad \mathbf{n} = \frac{-dy \mathbf{a}_x + dx \mathbf{a}_y}{\sqrt{dx^2 + dy^2}},$$

where \mathbf{a}_x and \mathbf{a}_y are the Cartesian basis vectors. The gradient vector is $\nabla T = \mathbf{a}_x$, while the right-hand side is $-x^4$. We therefore have a quadratic equation in dy/dx , which solves to give the boundary tracing ODE

$$(4.2) \quad \frac{dy}{dx} = \mp \frac{x^4}{\sqrt{1-x^8}}.$$

Note that traced boundaries do not exist in the region $x > 1$. The physical interpretation of this is that the known solution $T = x$ is not steep enough to carry a boundary flux of T^4 when $x > 1$.

There are two branches depending on the sign chosen for the square root. Integration yields traced boundaries of the form

$$(4.3) \quad y = \text{const} \mp \frac{x^5}{5} {}_2F_1\left(\frac{1}{2}, \frac{5}{8}; \frac{13}{8}; x^8\right),$$

shown in Figure 3, where ${}_2F_1$ is the hypergeometric function [12, Chapter 15]. The translational symmetry in the y -direction is a property inherited from the ODE (4.2). A local analysis near $x = 1$ shows that

$$(4.4) \quad y = \text{const} \pm \sqrt{\frac{1-x}{2}} + O(1-x)^{3/2},$$

and we see that the traced boundaries attach smoothly onto the straight line $x = 1$, which is itself a trivial traced boundary corresponding to the flat radiating face of Figure 2. Near $x = 0$ each pair of traced boundaries forms a thin cusp of the form

$$(4.5) \quad y = \text{const} \mp \frac{x^5}{5} + O(x^{13}).$$

Now each of the traced boundaries is a curve along which the radiation BC (3.3) is satisfied. More complicated boundaries can be constructed by patching together several of these curves, or portions thereof, and the only requirement is that there be consistent orientation. This requirement is satisfied by identifying as interior the side on which T (which equals x) is greater, i.e., the side to the right of each curve. Figure 4 shows a sample of the broad variety of radiation boundaries which can be produced in this manner. By construction, there are no singularities in the corners formed by the patching process. While the BC will not be satisfied at the corner points (due to the discontinuous normal), these points will contribute nothing to the integral of heat flux over the entire length of a constructed radiation boundary.

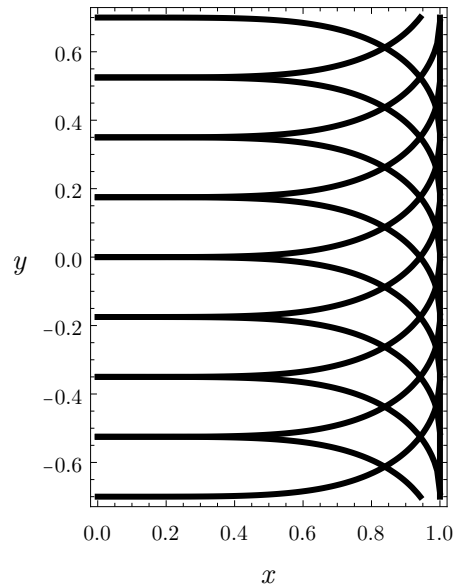


FIG. 3. *Traced boundaries (4.3).*

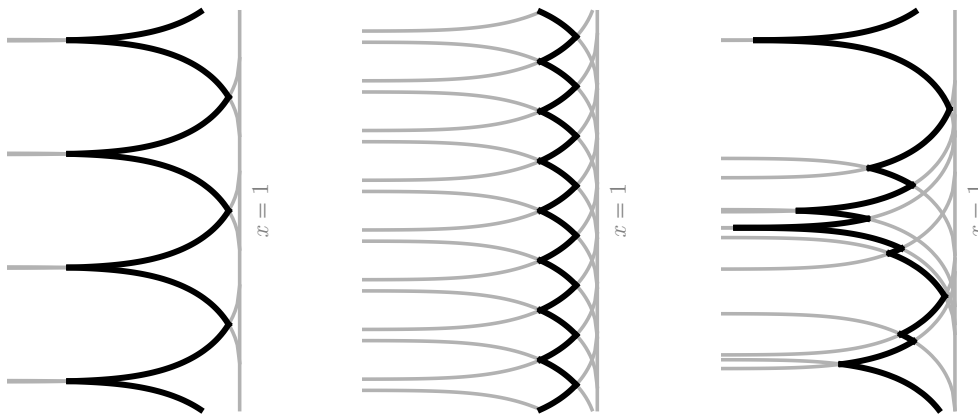


FIG. 4. *Radiation boundaries (thick black) patched together using the traced boundaries (4.3) (gray). Traced boundaries join smoothly onto the line $x = 1$.*

5. Domain construction. Since the constructed radiation boundaries only dissipate heat, a domain for the steady conduction–radiation BVP will not be completely specified until there is also a boundary to supply it. The simplest BC which can supply heat is the Dirichlet condition $T = \text{const}$, and given the form of the known solution (3.4), these boundaries are simply vertical lines, $x = \text{const}$.

An infinite number of conduction–radiation domains may therefore be marked out by joining a constructed radiation boundary with an appropriate Dirichlet boundary $x = \text{const}$, as in Figure 5. Each of these domains corresponds to steady conduction in the interior, constant temperature along the right-hand side, and thermal radiation into vacuum to the left. Most surprising is that *all* of these domains admit the *same* known solution (3.4).

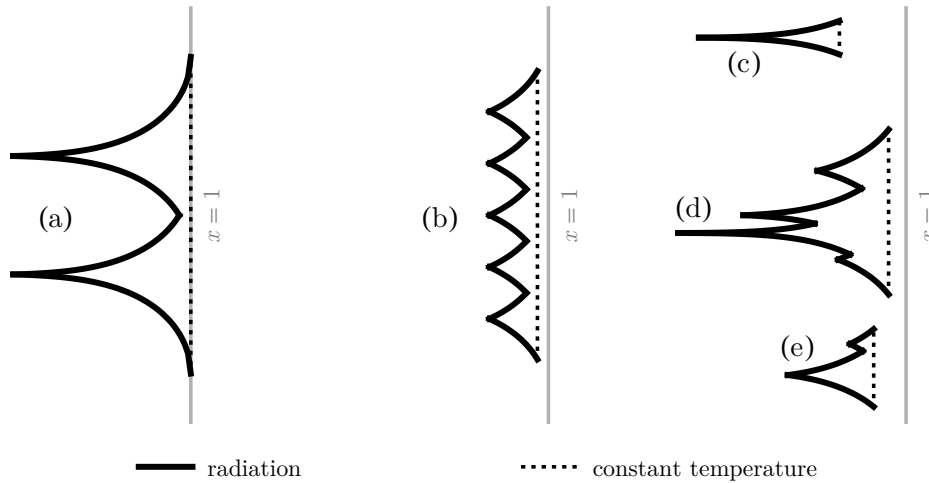


FIG. 5. Five domains (a)–(e) marked out by a radiation boundary and a constant temperature boundary. The straight line $x = 1$ is shown for reference.

From a mathematical perspective, the results we have just obtained using boundary tracing are *exact*. No approximation has been made in the solution to the field equation, nor in the determination of the radiation boundaries. However, the simple radiation BC (3.3) is not a complete description of the physics because the boundaries we have produced are not convex but *self-viewing*: some of the outgoing radiation travels not to infinity but strikes another part of the boundary, where it might be partially or fully absorbed. To correctly account for this behavior, the radiation BC would need to carry an additional term for inbound radiation emitted by self-viewing portions of the boundary.

6. Self-viewing fin. The technical issue of self-viewing radiation is unfortunate, but rather than immediately discard the results obtained, it is possible to quantify the amount of self-viewing radiation so that we might identify instances in which it is negligible. In Figure 5 we would expect considerable amounts of self-viewing exchange to occur for the domains (a), (b), (d), and (e) due to the adjacent spikes. Only for a single-spike domain such as (c) would we expect a small amount, so this is the case we consider here. While the analysis thus far has been in the xy -plane, the envisaged situation consists of a three-dimensional fin whose cross section is the domain (c). The analysis must necessarily be conducted in three dimensions, as radiation can be exchanged between points on the fin surface with different z .

Consider a differential area element dA at the local position $\mathbf{r} = x \mathbf{a}_x + y \mathbf{a}_y + z \mathbf{a}_z$, receiving radiation from a distant element dA^* at $\mathbf{r}^* = x^* \mathbf{a}_x + y^* \mathbf{a}_y + z^* \mathbf{a}_z$, as shown in Figure 6. We denote the displacement from \mathbf{r}^* to \mathbf{r} by

$$(6.1) \quad \mathbf{d}^* = \mathbf{r} - \mathbf{r}^*$$

and, respectively, let θ and θ^* be the angles that the normals \mathbf{n} and \mathbf{n}^* make with this displacement. Writing T and T^* for the temperatures of the two elements, the total power emitted by dA^* is (in scaled terms) $T^{*4} dA^*$. Almost none of this will strike the element dA . Indeed it is well known [7] that the *view factor* from dA^* to dA , defined as the fraction of radiation which leaves dA^* and strikes dA , is given by

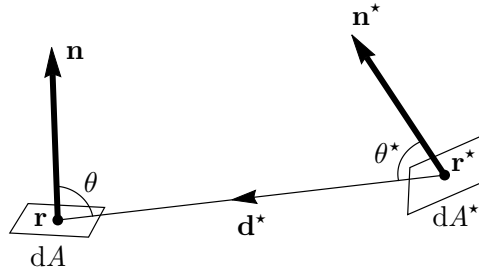


FIG. 6. Geometry of the area element \$dA\$ receiving radiation from the element \$dA^*\$.

$$(6.2) \quad \text{View factor} = \frac{\cos \theta^* \cos \theta \, dA}{\pi d^{*2}},$$

where \$d^* = \|\mathbf{d}^*\|\$. It follows that the amount of radiative power arriving at \$dA\$ is

$$(6.3) \quad \text{Power} = \frac{T^{*4} \cos \theta^* \cos \theta \, dA \, dA^*}{\pi d^{*2}}.$$

Assuming that all of this is absorbed by \$dA\$, we see that the radiation BC (3.3) must be modified to

$$(6.4) \quad \mathbf{n} \cdot \nabla T = -T^4 + \int \frac{T^{*4} \cos \theta^* \cos \theta \, dA^*}{\pi d^{*2}}$$

in order to account for self-viewing radiation.² The integral is to be taken over all elements \$dA^*\$ which can see the element \$dA\$ at the local position \$\mathbf{r}\$. The ratio

$$(6.5) \quad R = \frac{1}{T^4} \int \frac{T^{*4} \cos \theta^* \cos \theta \, dA^*}{\pi d^{*2}}$$

between the new integral term (for incoming radiation) and the existing quartic term (for outgoing radiation) provides a measure of whether self-viewing radiation is negligible for the domains we have produced using boundary tracing.

In the case of a single concave fin, shaped as \$y = y(x)\$ on \$x_1 \le x \le x_2\$ (Figure 7), it may be shown that (6.5) becomes

$$(6.6) \quad R = \frac{1}{T^4} \int_{x_1}^{x_2} \frac{T^{*4} [-(x - x^*)y'^* + (y - y^*)] [(x - x^*)y' - (y - y^*)] \, dx^*}{2[(x - x^*)^2 + (y - y^*)^2]^{3/2} \sqrt{1 + y'^2}},$$

where primes denote \$x\$-differentiation. Details are given in the first author's thesis [9, Appendix A.1]. Numerical evaluation of this integral may be easily performed given the expressions (4.2) and (4.3) for \$y'\$ and \$y\$, and the results are shown in Figure 8. While self-viewing radiation certainly cannot be neglected if \$x_1 = 0\$ or \$x_2 = 1\$, the self-viewing ratio \$R\$ may be significantly reduced by avoiding these two extremities. There are plenty of choices which ensure that the amount of self-viewing radiation is negligible in practice (\$R < 1\%\$). Generally speaking, we will decrease \$R\$ by shifting

²Since the integral term in (6.4) is *nonlocal*, self-viewing radiation cannot be analyzed using the method of boundary tracing, which requires a local flux condition of the form (2.1).

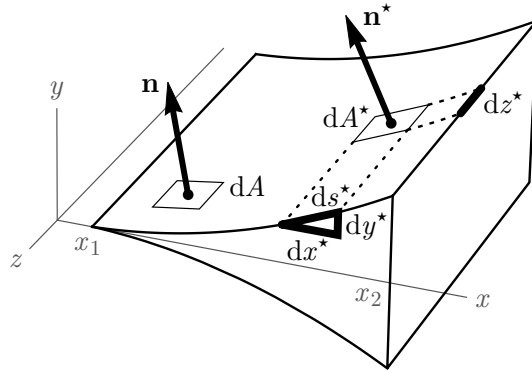


FIG. 7. Geometry of the area elements dA and dA^* in a self-viewing concave fin constructed from traced boundaries on $x_1 \leq x \leq x_2$.

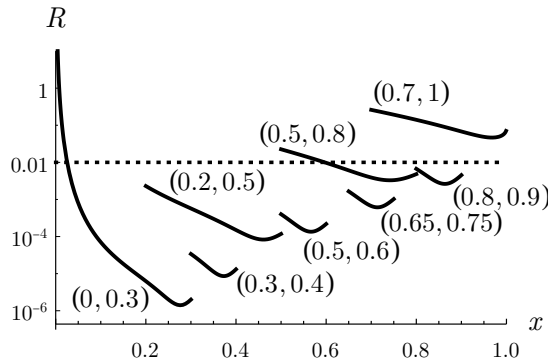
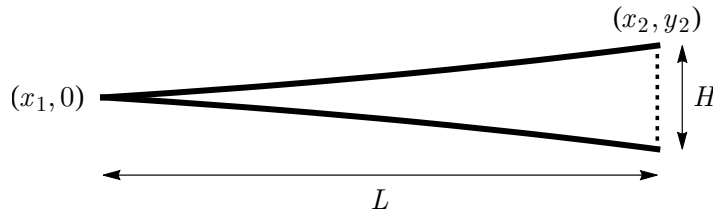


FIG. 8. Self-viewing ratio (6.6) for various fin endpoints (x_1, x_2) . The threshold value shown is 1% (dotted).

the chosen interval toward $x = 0$, although this is not surprising given that the traced boundaries have less curvature toward the left end (recall Figure 3). Alternatively we may decrease R by reducing the length $x_2 - x_1$ of the interval (but we note that the temperature variation in the fin will simultaneously be reduced). In either case, a decrease in R will bring the fin closer to the limiting case of a triangular fin, which has zero self-viewing radiation.

7. Physical example. Our analysis up to this point has been conducted in dimensionless variables. It is not immediately clear if our results are useful in practice, as the temperature and length scales Θ and λ (i.e., (3.1) and (3.2)) depend parametrically on both the radiation constant c and the slope h of the one-dimensional solution (2.2). For a given choice of material (having emissivity ϵ and conductivity k), the value of c is fixed by (1.3); only h can be varied freely. To assess whether this single degree of freedom allows us to achieve reasonable temperatures and lengths in practical applications, we construct here an explicit physical example (in unscaled variables) of the self-viewing fin of Figure 7. Here we restore the hats which were dropped after scaling.

Suppose we want a fin roughly 5 times as long (in the x -direction) as it is thick (in the y -direction). Its half-thickness should therefore be roughly a tenth of its length.

FIG. 9. *Physical fin dimensions.*

Since

$$\left. \frac{dy}{dx} \right|_{\hat{x}=0.55} = \left. \frac{d\hat{y}}{d\hat{x}} \right|_{\hat{x}=0.55} = \mp 0.092 \approx \mp 0.1,$$

we see that the desired aspect ratio can be approximately achieved by choosing a small x -interval centered on $\hat{x} = 0.55$, e.g.,

$$(7.1) \quad (\hat{x}_1, \hat{x}_2) = (0.5, 0.6).$$

In unscaled terms, the fin has length

$$(7.2) \quad L = x_2 - x_1 = (\hat{x}_2 - \hat{x}_1)\lambda = 0.1\lambda$$

and thickness

$$(7.3) \quad H = 2y_2 = 2\hat{y}_2\lambda = 0.0187\lambda$$

as shown in Figure 9. For our choice of endpoints, the self-viewing ratio (6.6) evaluates to less than 5×10^{-4} . Thus we may safely disregard self-viewing radiation in the results to follow.

From our scales (3.1) and (3.2), we have

$$(7.4) \quad \Theta = \left(\frac{1}{c\lambda} \right)^{1/3} = \left(\frac{\hat{x}_2 - \hat{x}_1}{cL} \right)^{1/3},$$

and therefore

$$(7.5) \quad T = \hat{T}\Theta = \hat{x}\Theta = \hat{x} \left(\frac{\hat{x}_2 - \hat{x}_1}{cL} \right)^{1/3}$$

for the physical temperature along the fin. Evaluating at \hat{x}_2 and \hat{x}_1 gives the temperature at the base and the tip, respectively. Figure 10(a) shows the corresponding Celsius temperatures³ for an anodized aluminium fin with emissivity $\epsilon = 0.9$ [15, Figure 4] and conductivity $k = 236 \text{ W m}^{-1} \text{ K}^{-1}$ [6, Figure 1]. For a fin of length $L = 1 \text{ m}$ (and hence thickness $H = 0.19 \text{ m}$), these evaluate to 191°C at the base and 114°C at the tip, which are quite reasonable as temperatures in an engineering context. A longer fin with a lower temperature might find application as a heat sink on a spacecraft. Thus boundary tracing is not merely an esoteric exercise; highly practical results can be obtained.

³Given an absolute temperature T , the corresponding Celsius temperature is $t = T - 273.15 \text{ K}$ so that $t/^\circ\text{C} = T/\text{K} - 273.15$.

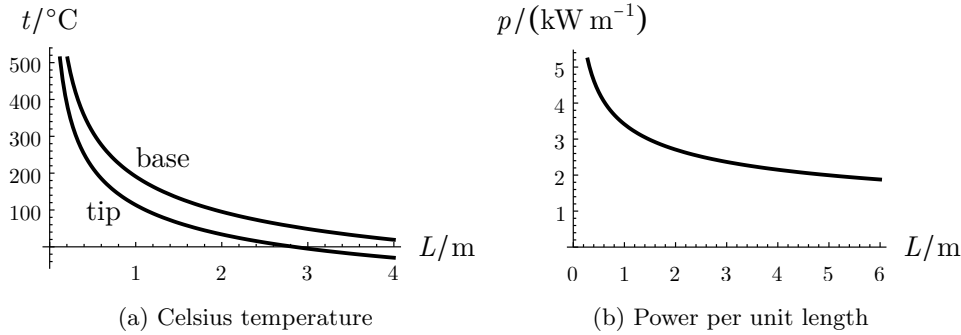


FIG. 10. Physical quantities as a function of the fin length L for an anodized aluminium fin with scaled endpoints (7.1).

The physical rate of heat transfer may be estimated similarly. The heat flux of the one-dimensional known solution is

$$(7.6) \quad -k \nabla T = -\frac{k\Theta}{\lambda} \hat{\nabla} \hat{T} = -\frac{k\Theta}{\lambda} \mathbf{a}_x,$$

a constant vector, representing the power dissipated in the negative x -direction per unit area in the yz -plane. Multiplying its magnitude by the fin thickness $H = 2\hat{y}_2\lambda$ yields

$$(7.7) \quad p = 2\hat{y}_2 k\Theta = 2\hat{y}_2 k \left(\frac{\hat{x}_2 - \hat{x}_1}{cL} \right)^{1/3}$$

for the power dissipated per unit z -length. The resulting curve for anodized aluminium is displayed in Figure 10(b), and for a fin of length $L = 1 \text{ m}$, we obtain $p = 3.41 \text{ kW m}^{-1}$.

8. Directional distribution. Lastly, we note that the directional distribution of radiation emitted from a fin will be significantly different to that from a simple rectangular strip. We consider the amount of radiation arriving at a cylindrical shell (aligned with the z -axis) of radius ρ (assumed large). Following a similar analysis to the earlier self-viewing calculations, we find that, in the case of a fin (Figure 11(a)), the radiative power per unit area received by the cylindrical shell is

$$(8.1) \quad I = \frac{1}{2\rho} \int_{x_1}^{x_2} \epsilon\sigma T^{*4} (y'^* \cos \varphi + \sin \varphi) dx^*,$$

where φ is the angle from the negative x -axis. Only a small amount of the radiative output is sent in the $\varphi = 0$ -direction (in which the fin points), with the majority of the radiation instead emitted laterally (perpendicular to the two faces of the fin). In contrast, for a rectangular strip in the yz -plane (Figure 11(b), similar to the radiating face of the slab in Figure 2), we have the cosinusoidal distribution

$$(8.2) \quad I = \frac{1}{2\rho} \epsilon\sigma T^4 H \cos \varphi,$$

where T is the temperature of the strip and H is its thickness in the y -direction. The normalized distributions are shown in Figure 12, where the fin distribution (8.1) has

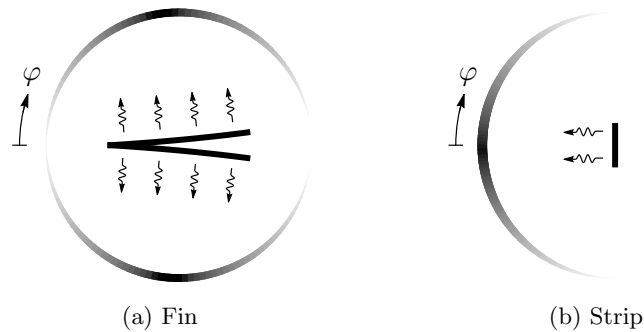


FIG. 11. *Directional distribution of radiative output for different shapes. Darker portions (along the outer ring) indicate more radiation.*

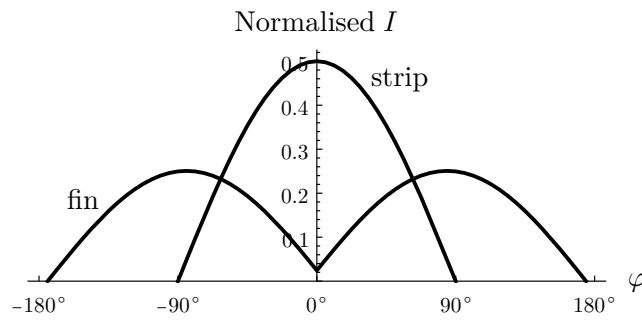


FIG. 12. *Normalized directional distribution of radiative output for a fin with scaled endpoints (7.1) and for a rectangular strip.*

been explicitly evaluated for our earlier fin example. As expected, the strip emits most of its radiative output in the direction that it faces. This may not be desirable, and the fin provides a useful alternative in applications where laterally emitted radiation is preferred.

9. Conclusions. Boundary tracing is an alternative approach that allows for the analytical study of flux BVPs when conventional techniques fail. Using a simple one-dimensional solution to Laplace's equation, we have applied the method of boundary tracing to obtain an infinite family of nontrivial radiation boundaries for a conduction–radiation BVP. This has enabled us to produce a multitude of new domains that admit the chosen solution. While the technical issue of self-viewing radiation has prevented us from labeling these as exact results, we have identified fin-shaped domains for which the amount of self-viewing radiation is negligible. Such domain shapes are of practical interest in the space radiation context, and our analysis has shown that the associated length and temperature scales are in the practically interesting range.

Of course the one-dimensional solution is not the only solution to Laplace's equation; we are free to choose any known solution to the field equation for the purposes of boundary tracing. By starting with sinusoidal solutions and line-source solutions, it is possible to construct a vast array of convex conduction–radiation domains (which do not suffer from the issue of self-viewing radiation), including lens-shaped, polygon-like,

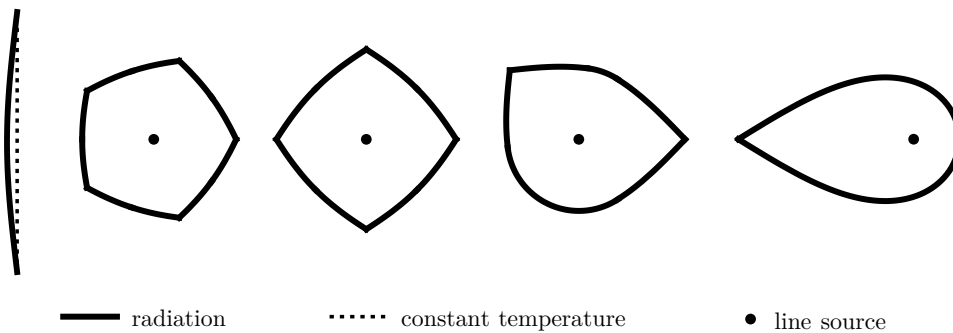


FIG. 13. Assorted conduction–radiation domains constructed using boundary tracing.

and teardrop-shaped regions. Selected examples are shown in Figure 13, and we refer the reader to the first author’s thesis [9] for extended analysis.

Finally, the boundary tracing approach does not require linearity in either the field equation or the flux BC. However, in cases where the field equation happens to be linear, we are free to make exact perturbations of the known solution. For the fin-shaped domains identified earlier, it is conceivable that suitable perturbations of the known solution might nudge the nonconvex radiation boundaries into convex ones (hence eliminating the unfortunate issue of self-viewing radiation). Such a technique could extend the results obtained here; more generally it could be used to investigate subtle change of boundary shape for any flux BVP where the underlying field equation is linear.

Acknowledgments. We thank the anonymous referees, whose input has led to an improved paper.

REFERENCES

- [1] M. L. ANDERSON, A. P. BASSOM, AND N. FOWKES, *Exact solutions of the Laplace–Young equation*, Proc. Roy. Soc. A, 462 (2006), pp. 3645–3656, <https://doi.org/10.1098/rspa.2006.1744>.
- [2] M. L. ANDERSON, A. P. BASSOM, AND N. FOWKES, *Boundary tracing and boundary value problems: I. Theory*, Proc. Roy. Soc. A, 463 (2007), pp. 1909–1924, <https://doi.org/10.1098/rspa.2007.1858>.
- [3] M. L. ANDERSON, A. P. BASSOM, AND N. FOWKES, *Boundary tracing and boundary value problems: II. Applications*, Proc. Roy. Soc. A, 463 (2007), pp. 1925–1938, <https://doi.org/10.1098/rspa.2007.1859>.
- [4] J. G. BARTAS AND W. H. SELLERS, *Radiation fin effectiveness*, J. Heat Transfer, 82 (1960), pp. 73–75, <https://doi.org/10.1115/1.3679882>.
- [5] R. L. CHAMBERS AND E. V. SOMERS, *Radiation fin efficiency for one-dimensional heat flow in a circular fin*, J. Heat Transfer, 81 (1959), pp. 327–329, <https://doi.org/10.1115/1.4008219>.
- [6] J. G. COOK, J. P. MOORE, T. MATSUMURA, AND M. P. VAN DER MEER, *The Thermal and Electrical Conductivity of Aluminum*, Tech. Report ORNL-5079, Oak Ridge National Laboratory, 1975, <https://doi.org/10.2172/5066461>.
- [7] J. R. HOWELL, R. SIEGEL, AND M. P. MENGÜÇ, *Thermal Radiation Heat Transfer*, 5th ed., CRC Press, Boca Raton, FL, 2010.
- [8] H. H. KELLER AND E. S. HOLDREDGE, *Radiation heat transfer for annular fins of trapezoidal profile*, J. Heat Transfer, 92 (1970), pp. 113–116, <https://doi.org/10.1115/1.3449597>.
- [9] C. LI, *Applications of Boundary Tracing in Thermal Radiation and Capillarity*, Ph.D. thesis, University of Western Australia, 2021, <https://doi.org/10.26182/f2wk-c635>.
- [10] S. LIEBLEIN, *Analysis of Temperature Distribution and Radiant Heat Transfer Along a Rectangular Fin of Constant Thickness*, Tech. Report D-196, National Aeronautics and Space Administration, 1959, <https://archive.org/details/nasa.techdoc.19890068385>.

- [11] C.-Y. LIU, *On minimum-weight rectangular radiating fins*, J. Aerosp. Sci., 27 (1960), pp. 871–872, <https://doi.org/10.2514/8.8784>.
- [12] F. W. J. OLVER, D. W. LOZIER, R. F. BOISVERT, AND C. W. CLARK, EDS., *NIST Handbook of Mathematical Functions*, Cambridge University Press, Cambridge, UK, 2010.
- [13] A. R. SHOUMAN, *An exact general solution for the temperature distribution and the composite radiation convection heat exchange along a constant cross-sectional area fin*, Quart. Appl. Math., 25 (1968), pp. 458–462, <https://doi.org/10.1090/qam/99882>.
- [14] E. TIESINGA, P. J. MOHR, D. B. NEWELL, AND B. N. TAYLOR, *The 2018 CODATA Recommended Values of the Fundamental Physical Constants*, web version 8.1, 2019, <https://physics.nist.gov/cuu/Constants/>, accessed April 14, 2020.
- [15] P. WADE AND C. PREEDY, *Fujihokka: A high-emissivity approach to aluminum anodizing*, Metal Finish., 101 (2003), pp. 8–13, [https://doi.org/10.1016/S0026-0576\(03\)90093-6](https://doi.org/10.1016/S0026-0576(03)90093-6).
- [16] J. E. WILKINS, JR., *Minimum-mass thin fins which transfer heat only by radiation to surroundings at absolute zero*, J. Soc. Ind. Appl. Math., 8 (1960), pp. 630–639, <https://doi.org/10.1137/0108047>.
- [17] J. E. WILKINS, JR., *Minimum mass thin fins with specified minimum thickness*, J. Soc. Ind. Appl. Math., 9 (1961), pp. 194–206, <https://doi.org/10.1137/0109019>.
- [18] J. E. WILKINS, JR., *Minimum-mass thin fins and constant temperature gradients*, J. Soc. Ind. Appl. Math., 10 (1962), pp. 62–73, <https://doi.org/10.1137/0110006>.
- [19] J. E. WILKINS, JR., *Optimum shapes for fins rejecting heat by convection and radiation*, J. Franklin Inst., 297 (1974), pp. 1–6, [https://doi.org/10.1016/0016-0032\(74\)90133-1](https://doi.org/10.1016/0016-0032(74)90133-1).